ISSN 1870-4069

Spatio-Spectro-Temporal Characterization of Ultrashort Vortex Pulses

Erick R. Baca-Montero, Oleksiy V. Shulika

Universidad de Guanajuato,
Departamento de Ingeniería Eléctrica,
Mexico

{er.bacamontero, oshulika}@ugto.mx

Abstract. Due to the promising features of optical vortices a variety of methods have been developed for their generation, however, these methods are mostly intended for CW vortex beams and thus can be hardly usable for generation of ultrashort vortex pulses. A spiral phase plate (SPP) is a robust method for vortex generation with potential to be used in ultrafast optics, however, the resulting vortex is not a pure vortex mode but contains contributions of different radial orders. As well, the SPP exhibits a wavelength-dependent phase shift, due to its material dispersion. Here we present a (3+1)D numerical analysis of the spatio-spectro-temporal properties of ultrashort vortex pulses generated with spiral phase plates characterizing the effects of material dispersion and propagation geometry. These results can serve as a basis for the design of new passive and active devices for singular optics and photonics.

Keywords: Spatio-spectro-temporal characterization, ultrashort vortex pulses, spiral phase plate (SPP), laguerre–gaussian (LG) modes, material dispersion.

1 Introduction

Ultrashort vortex pulses are electromagnetic radiation with durations in the order of picoseconds or less (broadband optical spectrum) and that present points where the intensity of the wave is zero around the axis of the beam and the phase is undefined [1]. In recent years the study of vortex pulses has peaked due to their promising features in super-resolution microscopy [7], optical tweezers [6], ultra-fast optical communications [3], quantum computing [9] and astrophysics [4]. Laguerre–Gaussian (LG) modes are the most commonly studied set of vortices. They are derived by solving the paraxial Helmholtz equation in cylindrical coordinates [1]. An LG pulse is given by:

$$u_{p,l}^{LG}(r,\phi,z,t) = \underbrace{\frac{C_{lp}^{LG}}{w(z)}\left(\frac{r\sqrt{2}}{w(z)}\right)^{|l|} L_p^{|l|}\left(\frac{2r^2}{w^2(z)}\right) e^{-\frac{r^2}{w^2(z)}} e^{\frac{-ikr^2}{2\left(z^2+z_R^2\right)}} e^{-il\phi} e^{(i(2p+l+1)\psi)}}_{\text{Laguerre Gaussian Mode Factor}} \underbrace{e^{\frac{-(t-t_0)}{\tau^2}} e^{i\omega_t t}}_{\text{Temporal Profile factor}}. \quad (1)$$

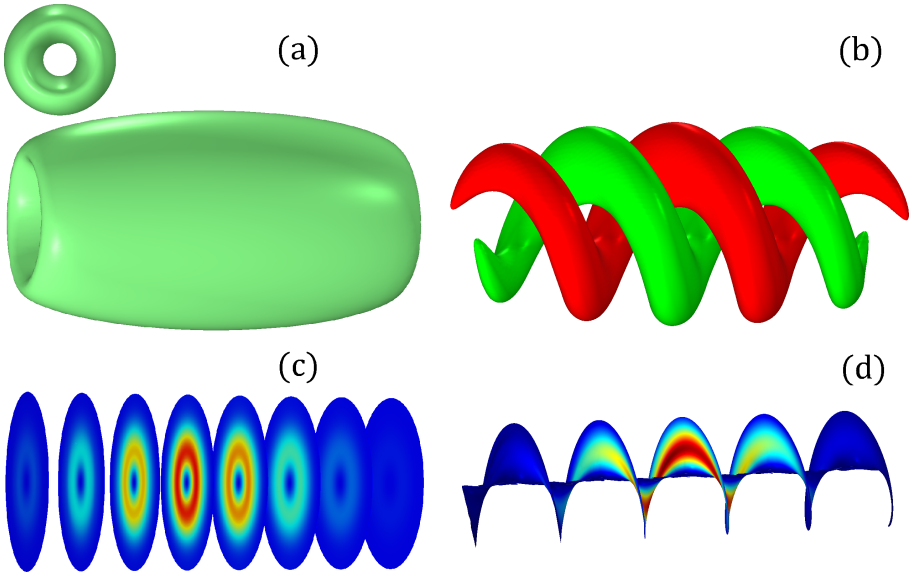

Fig. 1. 3D vortex pulse $LG_{0,1}$ with a duration $\tau = 5\,\text{fs}$: (a) Spatio-temporal intensity profile isosurface set at half of the peak intensity. (b) Isosurfaces of the real part of the complex field. (c) Slices of the characteristic doughnut spatial intensity profile of the vortex pulse along. (d) Isosurface of the spiraling phase of the vortex pulse.

Here w_0 is the beam radius at the beam waist, r is the radial distance from the center axis of the beam, z_R is the Rayleigh range, ψ is the Gouy phase, $R(z)$ is the radius of curvature, C_{lp}^{LG} is a normalization constant [1], $L_p^{|l|}$ is the generalized Laguerre polynomial of order p and l, and $w(z)$ is the radius of the beam at a given position z, l is called topological charge and it defines the azimuthal distribution (the amplitude has azimuthal angular dependence, $e^{-il\phi}$) that can be positive or negative indicating left or right circulation, while p defines the radial distribution index.

In the temporal factor τ is the duration of the pulse, t_0 is the pulse center time and ω_t is the central angular frequency. A LG mode retains its intensity profile upon propagation, although with a different width and the Gouy phase changes by multiples $(2p + |l| + 1)\pi/2$ as it travels. For $l = 0$, $p = 0$, the expression eq. 1 reduces to that of an ordinary Gaussian beam, as $L_p^{|l|} = 1$. Because l is an integer, the phase of the field can only increase or decrease by multiples of 2π as one follows a closed path around the axis of the beam.

The radial distribution p gives a number of dark rings nested in the beam profile. Figure 1 shows a three-dimensional reconstruction of the vortex pulse $LG_{0,1}$ with a duration $\tau = 5\,\text{fs}$ The characteristic zero intensity point at the vortex axis can be observed in figures 1 (a) and (c) which show the spatio-temporal intensity profile $|u(x, y, t)|^2$ and slices through the centre of the beam, respectively. The spiraling nature can be observed in figures 1 (b) and (d) which show isosurfaces of the real part of the complex field, $\Re\,|u(x, y, t)|$ and of the phase (Here the color scale shows the spatio-temporal intensity profile of the vortex pulse along spiraling phase).

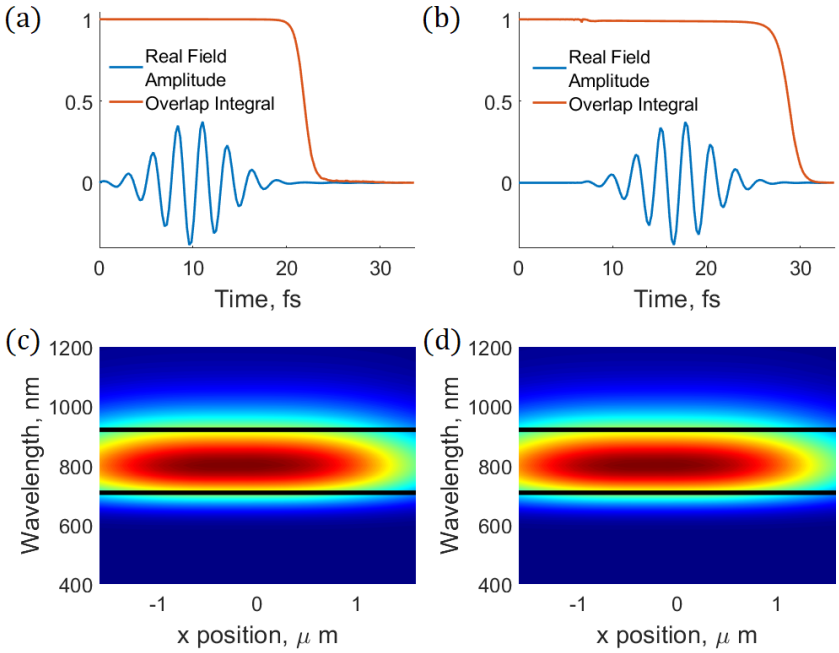

Fig. 2. Spatio-spectro-temporal properties of a vortex pulse upon dispersive propagation in 2λ long SiO_2 block: (a) Real field amplitude of the input vortex pulse and overlap integral (b) Real field amplitude of the vortex pulse and overlap integral after propagation (c) Spatially resolved spectral intensity of the input vortex pulse. (d) Spatially resolved spectral intensity of the output vortex pulse.

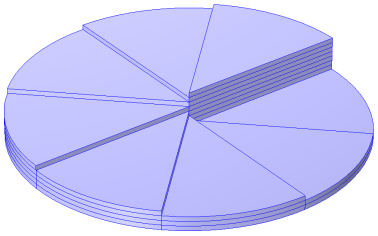

Fig. 3. Schematic of a 8-levels discrete SPP.

2 Ultrashort OVs Spatio-Spectro-Temporal Characterization During Propagation and Generation with a Spiral Phase Plate

In this work, the propagation and generation of ultrashort vortex pulses is analyzed using control parameters calculated at the input and output of the model domain, these are the real field value of the electric field, the electric field intensity, the spatially resolved spectral intensity and OI_I the overlap integral between the amplitude of the analytic LG01 mode (eq. 1) and its numerical counterpart (u_{num}).

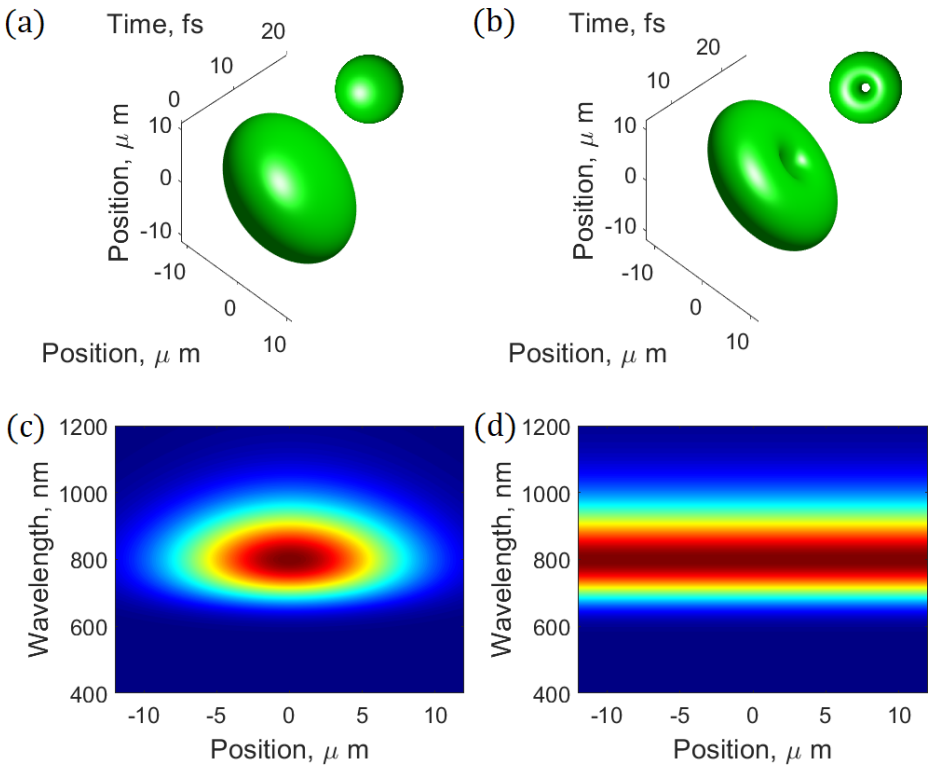

Fig. 4. Spatio-spectro-temporal properties of input pulse to a SPP and of the generated vortex pulse: (a) Spatio-temporal intensity profile isosurface set at half of the peak intensity of the input gaussian pulse. (b) Spatio-temporal intensity profile isosurface set at half of the peak intensity of the generated vortex pulse. (c) Spatially resolved spectral intensity of the input gaussian pulse. (d) Spatially resolved spectral intensity of the generated vortex pulse.

The overlap integral is given as:

$$OI_I = \frac{\left| \int u_{0,1}^{\mathrm{LG}} * u_{\mathrm{num}} dA \right|^2}{\int \left| u_{0,1}^{\mathrm{LG}} \right|^2 dA \int \left| u_{\mathrm{num}} \right|^2 dA}. \tag{2}$$

And it gives the quality of vortex modes [2].

2.1 Propagation of Ultrashort Vortex Pulses in Dispersive Media

The characteristics of a $5\,\mathrm{fs}$ vortex pulse of wavlength $\lambda = 800\,\mathrm{nm}$ upon propagation in a dispersive SiO_2 block of thickness $t = 2\lambda$ are studied. The refractive index of the SiO_2 is given in [5]. Fig. 2 (a) and (b) show the real field amplitude and the overlap integrals (eq. 2) of the vortex before and after propagation, small temporal chirp is acquired (less than $1\,\mathrm{fs}$), while the spatial spectral intensity measured along a line at the

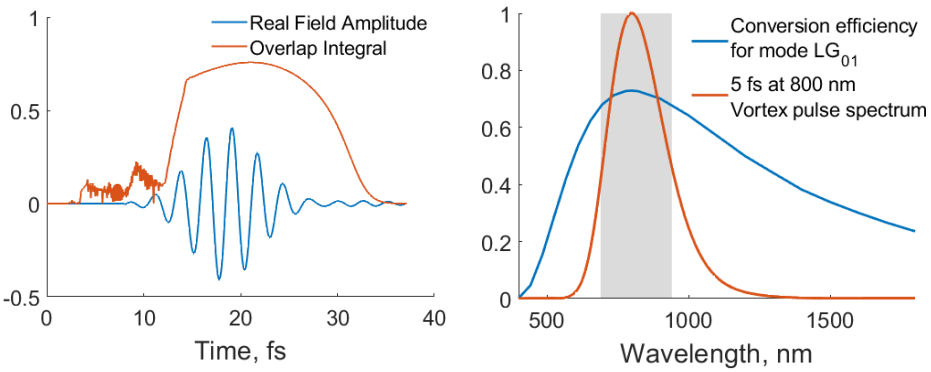

Fig. 5. (a) Temporal real field amplitude and overlap integral between analytic LG_{01} mode (eq. 1) and generated ultrashort vortex pulse. (b) Conversion efficiency dependence in wavelength for an 8-levels SPP and spectrum of a $5\,\mathrm{fs}$ vortex pulse at $\lambda = 800\,\mathrm{nm}$.

left side maximum of the vortex 2 (c) and (d) before and after propagation respectively, shows that the spectrum half amplitude remains constant and therefore the vortex does not present spatial chirp, furthermore, it is then possible to compensate for the time chirp through normal dispersion compensation techniques, as also shown in [8].

2.2 Ultrashort Vortex Generation with a Spiral Phase Plate

A Spiral Phase Plate (SPP) [2] is an optical component for the generation of vortex beams. In this device with refractive index n the optical thickness t is varied with an azimuthal angle ϕ according to:

$$t = \phi l \lambda / 2\pi (n - n_b), \tag{3}$$

where λ is the incident beam wavelength and n_b is the refractive index of the medium containing the SPP. Fig. 4 shows the spatio-spectro-temporal properties of the vortex pulse generated with an 8-levels SPP (fig. 3), the spectrum half amplitude (fig. 3 (c) and (d)) remains constant for the input gaussian pulse and the generated vortex pulse, thus there is no spatial chirp.

The SPP has maximum conversion efficiency (Overlap integral, eq. 2) of 0.73 (fig. 5 (a)), while it presents a conversion efficiency of more than 0.68 in the bandwidth of the pulse (from $700\,\mathrm{nm}$ to $930\,\mathrm{nm}$) (fig. 5 (b)).

3 Conclusions

In this work, vortex pulses propagation and generation was simulated solving a time-domain wave-equation. Chromatic dispersion induces temporal broadening of the vortex pulses while the spatial profile and spatio-spectral properties remained unchanged, thus conventional dispersion compensation techniques, can be used to compress back broadened vortices.

As well the effect of a SPP chromatic dispersion is negligible on the temporal profile of optical vortex pulses (very small broadening at the studied temporal and spectral range), while the spatial profile and spatio-spectral properties of the vortex remained unchanged. The analyzed SPP presents a conversion efficiency of more than 0.6 in a bandwidth from $630\,\mathrm{nm}$ to $1050\,\mathrm{nm}$. The results obtained in modeling vortex pulses can serve as a basis for novel devices design.

Acknowledgments. This work is supported by CONACyT via the PhD scholarship grant 763343 and by University of Guanajuato under research grant CIIC 272.2021.

References

1. Allen, L., Beijersbergen, M., Spreeuw, R. J. C.: Orbital angular momentum of light and the transformation of laguerre-gaussian laser modes. Physical Review A, vol. 45, no. 11, pp. 8185–8189 (1992) doi: 10.1103/physreva.45.8185
2. Beijersbergen, M. W., Coerwinkel, R. P. C., Kristensen, M., Woerdman, J. P.: Helical-wavefront laser beams produced with a spiral phaseplate. Optics Communications, vol. 112, no. 5-6, pp. 321–327 (1994) doi: 10.1016/0030-4018(94)90638-6
3. Bozinovic, N., Yue, Y., Ren, Y., Tur, M., Kristensen, P., Huang, H., Willner, A. E., Ramachandran, S.: Terabit-scale orbital angular momentum mode division multiplexing in fibers. Science, vol. 340, no. 6140, pp. 1545–1548 (2013) doi: 10.1126/science.1237861
4. Foo, G., Palacios, D. M., Swartzlander-Grover, A.: Optical vortex coronagraph. Optics Letters, vol. 30, no. 24, pp. 3308 (2005) doi: 10.1364/ol.30.003308
5. Malitson, I. H.: Interspecimen comparison of the refractive index of fused silica. Journal of the Optical Society of America, vol. 55, no. 10, pp. 1205 (1965) doi: 10.1364/josa.55.001205
6. Paterson, L., MacDonald, M. P., Arlt, J., Sibbett, W., Bryant, P. E., Dholakia, K.: Controlled rotation of optically trapped microscopic particles. Science, vol. 292, no. 5518, pp. 912–914 (2001) doi: 10.1126/science.1058591
7. Tamburini, F., Anzolin, G., Umbriaco, G., Bianchini, A., Barbieri, C.: Overcoming the rayleigh criterion limit with optical vortices. Physical Review Letters, vol. 97, no. 16 (2006) doi: 10.1103/physrevlett.97.163903
8. Toda, Y., Nagaoka, K., Shimatake, K., Morita, R.: Generation and spatiotemporal evolution of optical vortices in femtosecond laser pulses. Electrical Engineering in Japan, vol. 167, no. 4, pp. 39–46 (2009) doi: 10.1002/eej.20791
9. Wang, X. L., Luo, Y. H., Huang, H. L., Chen, M. C., Su, Z. E., Liu, C., Chen, C., Li, W., Fang, Y. Q., Jiang, X., Zhang, J., Li, L., Liu, N. L., Lu, C. Y., Pan, J. W.: 18-qubit entanglement with six photons' three degrees of freedom. Physical Review Letters, vol. 120, no. 26 (2018) doi: 10.1103/physrevlett.120.260502